Supporting Information

Deciphering effects of hexagonal and monoclinic structure distribution on properties of Li-rich layered oxides

Qingqing Ren[a,b], Huixian Xie[a], Minjun Wang[c], Xiaokai Ding[a], Jiaxiang Cui[a], Dong Luo[a,*], Chenyu Liu[a,*] and Zhan Lin[a]

a. School of Chemical Engineering and Light Industry, Guangdong University of Technology, Guangzhou 510006, China.

E-mail: luodong@gdut.edu.cn; cy.liu@gdut.edu.cn.

b. College of Chemistry and Material Science, Huaibei Normal University, Huaibei, 235000, Anhui, China.

c. Westlake University，Hangzhou, 310000, China.

Experimental Section

$(Mn_{0.75}Ni_{0.25})CO_3$ precursors were supplied by Anhui Fuli New Energy Technology Co., Ltd.

Synthesis of CLO sample

Manually mixing 1 g of $(Mn_{0.75}Ni_{0.25})CO_3$ precursors with 0.5182 g of $LiOH{\cdot}H_2O$, and then heating the mixture at 880 ^oC for 12 h with a heating ramp of 5 ^oC min^{-1} in muffle furnace (air atmosphere), the layered Li-rich Mn-based oxide was obtained as the control sample.

Synthesis of MLO sample

1 g of $(Mn_{0.75}Ni_{0.25})CO_3$ precursors were treated with 30 ml of ammonium hydroxide (5 M) by stirred for 20 min, then quickly filtered and washed for 7 times with distilled water. After dried at 60 ^oC for 8 h in an oven, the modified precursors were prepared and mixed with 0.5182 g of $LiOH{\cdot}H_2O$ to synthesize the Li-rich oxides as the

modified sample. The sintering process is the same as that of the control sample.

Material characterization

The information about element and structure of the samples is investigated by X-ray diffraction (a step width of 0.05°, Cu Kα radiation, Rigaku MiniFlex600), Raman Microscope (532 nm excitation laser, Renishaw inVia), photoelectron spectroscopy (Al X-ray source, K-Alpha, Thermo fisher Scientific), scanning (Hitachi-SU8220) and transmission (JEM-2100F) electron microscopy, and inductively coupled plasma optical emission spectroscopy (ICP-OES, PerkinElmer Optima 5300DV).

Electrochemical test

The electrochemical performance of the samples was evaluated by the half-cell configuration (CR-2032). The working electrodes were fabricated with a slurry of active materials, Super P, and polyvinylidene fluoride (8: 1: 1) in N-methy-2-pyrrolidone coated on Al foil. After dried at 120 °C for 12 h in vacuum, the loading mass of active materials was about 2 mg cm^{-2}. In an Ar-filled glovebox of water and oxygen contents below 0.1 ppm, the coin cells were assembled with electrolyte of 1 M $LiPF_6$ in ethylene carbonate, dimethyl carbonate, and ethylmethyl carbonate (1: 1 : 1 vol%), Li metal as the counter electrode and microporous polypropylene membrane (Celgard 2500) as the separator. The C-rates were calculated with considering 1 C as 200 mA g^{-1}. Below 1 C, galvanostatic charging-discharging operation was adopted. When equal or greater than 1 C, constant current and constant voltage (CCCV) charge was carried out with cut-off currents of 100 mA g^{-1} for constant voltage stages. The potential range is of 2.0 V - 4.7 V (LAND CT2001 testing system, China). During the galvanostatic intermittent titration technique testing (GITT), a constant current flux of 40 mA g^{-1} for 10 min was supplied, followed by open circuit conditions for 40 min. Cyclic voltammetry curves (CV) were recorded at scan rates of 0.1 mV s^{-1} (CHI760E, China). The frequency range of 100 KHz - 0.01 Hz was for electrochemical impedance spectroscopy (EIS) and the cell rested for 8 h before tested. Full cells were assembled with the fresh cathodes and pre-lithiated Si/C anodes. The pre-lithiated method is of 10 cycles at 0.2 A g^{-1} with a half-cell configuration. Electrochemical measurements were performed at room temperature.

Supplementary Figures

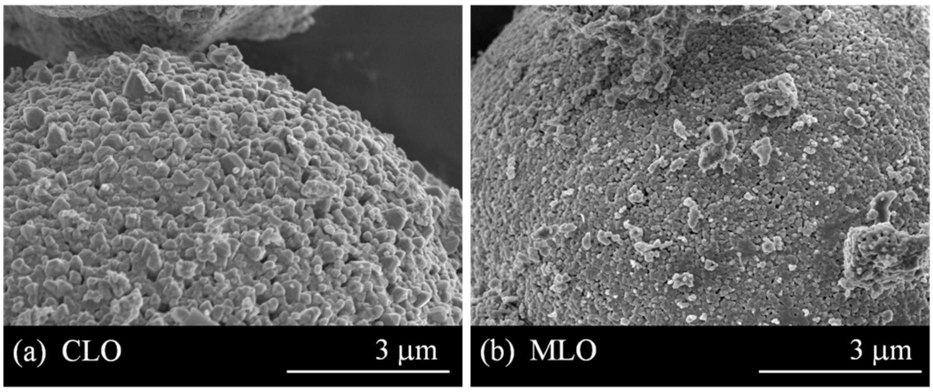

Fig. S1 SEM images of (a) CLO and (b) MLO samples.

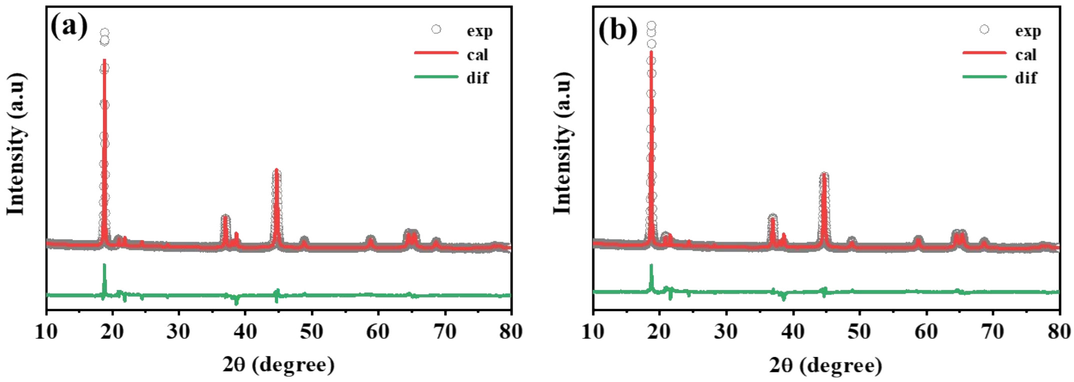

Fig. S2 Refined XRD patterns of (a) CLO and (b) MLO samples.

Table S1. Lattice parameter of $LiMO_2$ structure in CLO and MLO samples.

Sample	*a* (Å)	*c* (Å)
CLO	2.8612(1)	14.1641(1)
MLO	2.8633(2)	14.286(1)

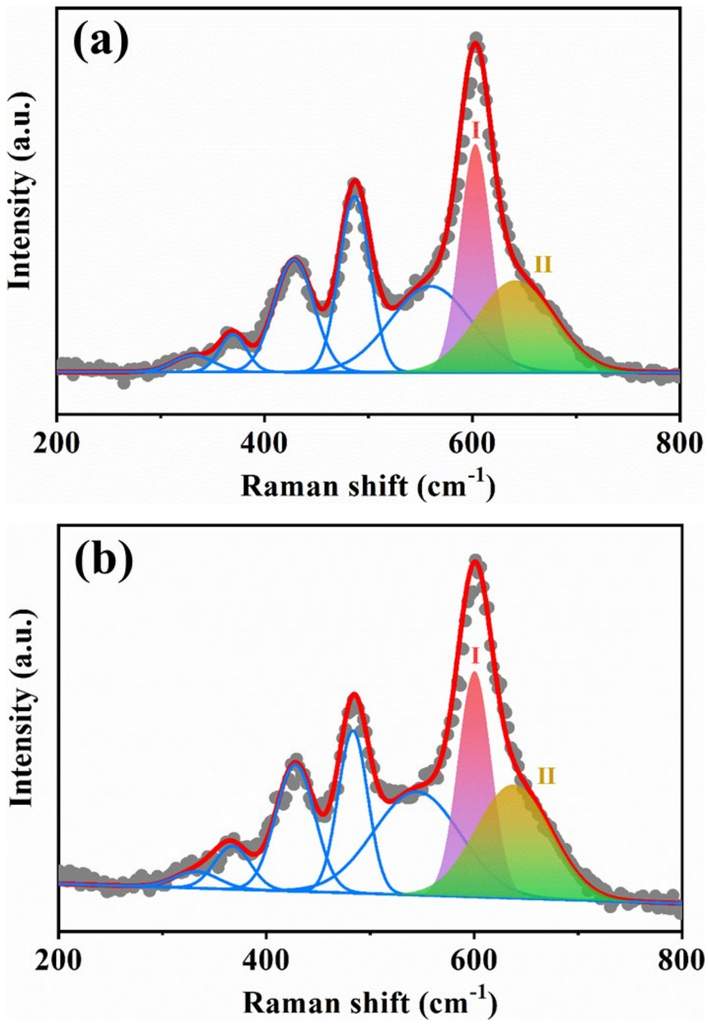

Fig. S3 The fitting Raman spectra of (a) MLO and (b) CLO samples.

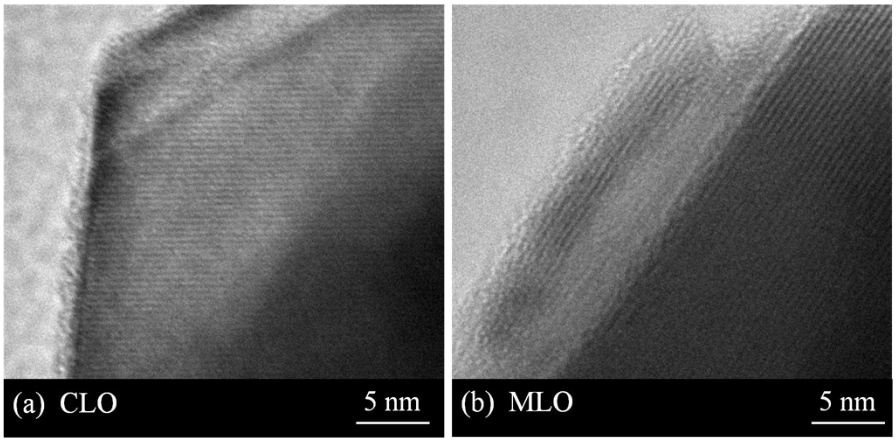

Fig. S4 HRTEM images of the fresh (a) CLO and (b) MLO samples.

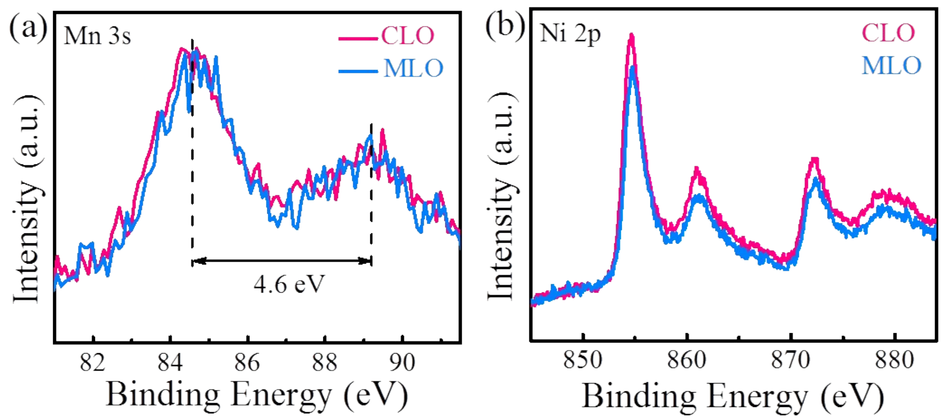

Fig. S5 (a) Mn 3s and (b) Ni 2p XPS spectra for CLO and MLO samples collected after storing 90 days.

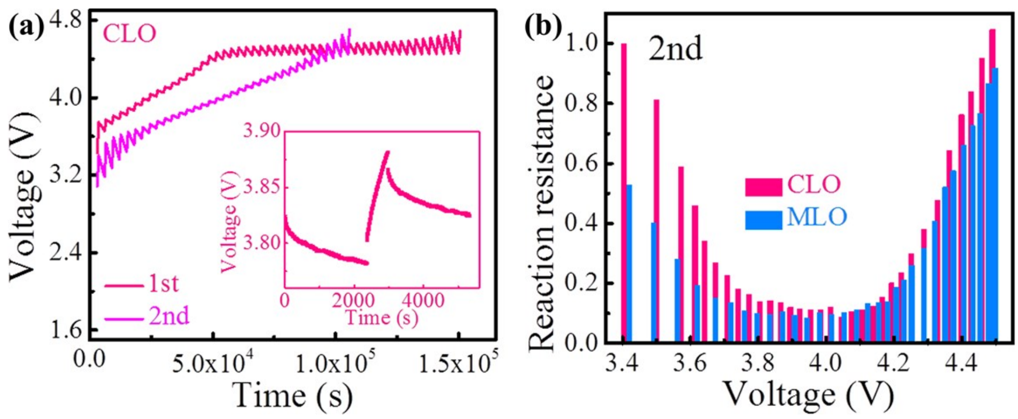

Fig. S6 (a) GITT curves of the first and second charging for CLO cathode, the inset is a single titration; And (b) the calculated reaction resistance of the 2nd charge process based on the GITT curves.

The corresponding diffusion coefficient of Li^+ was calculated by GITT curves with the following equation. A represents electrode surface. M, V_M, and m is the molar mass, molar volme, and mass of $Li_{1.2}Mn_{0.6}Ni_{0.2}O_2$, respectively.

$$D_{Li^+} = \frac{4}{\pi}\left(\frac{mV_M}{MA}\right)^2\left(\frac{\Delta Es}{\Delta E\tau}\right)^2$$

As shown in Fig. S7, there is no obvious difference in Li^+ diffusion coefficient between CLO and MLO during the initial activation process.

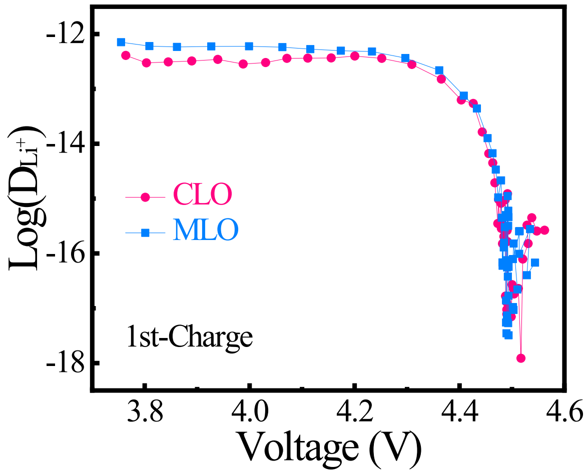

Fig. S7 Li^+ diffusion coefficient calculated from GITT measurements for CLO and MLO during the initial charging process.

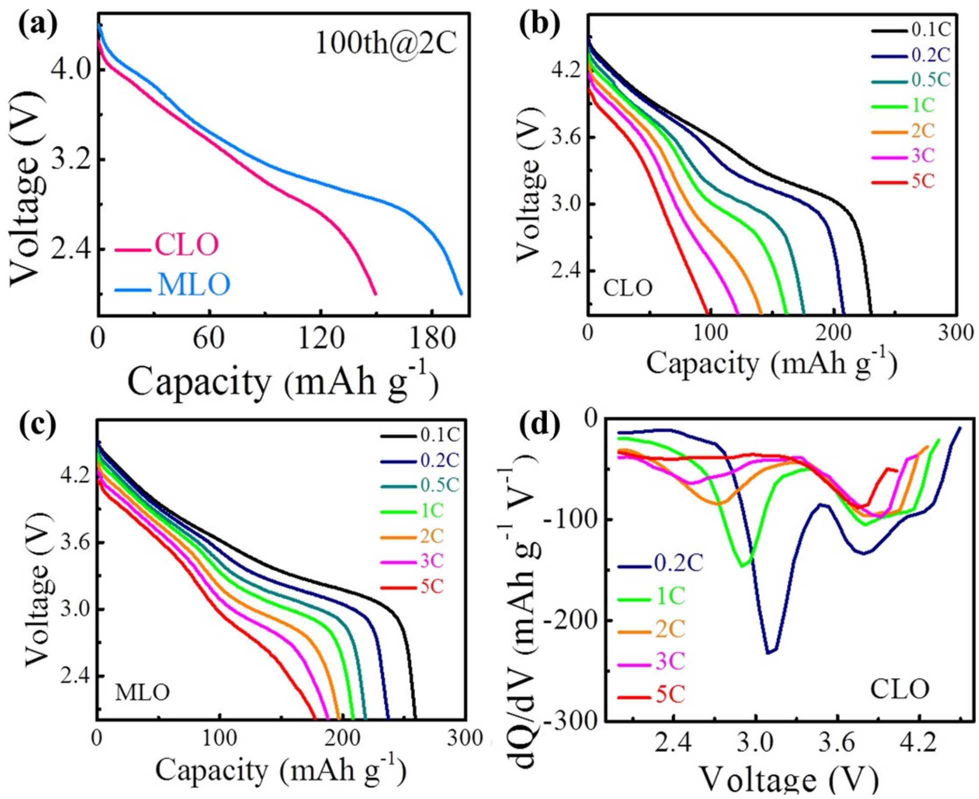

Fig. S8 (a) the 100[th] discharge profiles, discharge profiles at various rates of (b) CLO and (c) MLO cathodes, and (d) corresponding dQ/dV curves of CLO sample.

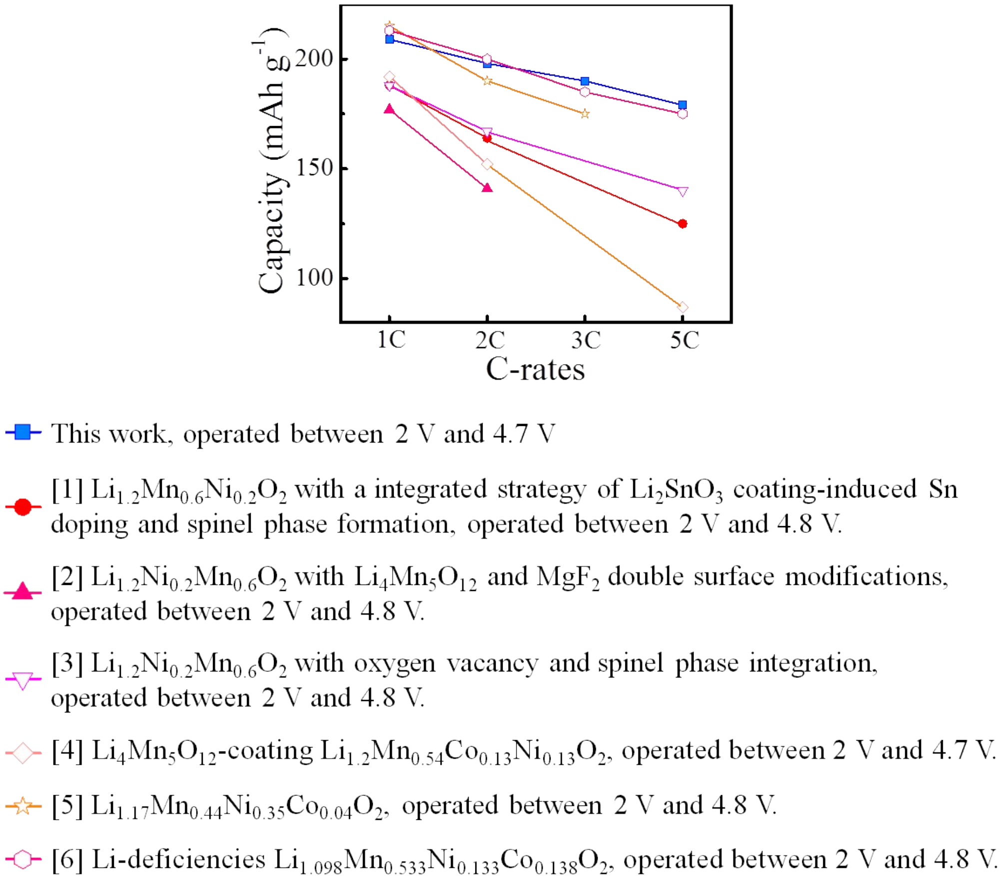

Fig. S9 High-rate performance comparison between the modified cathode and others.

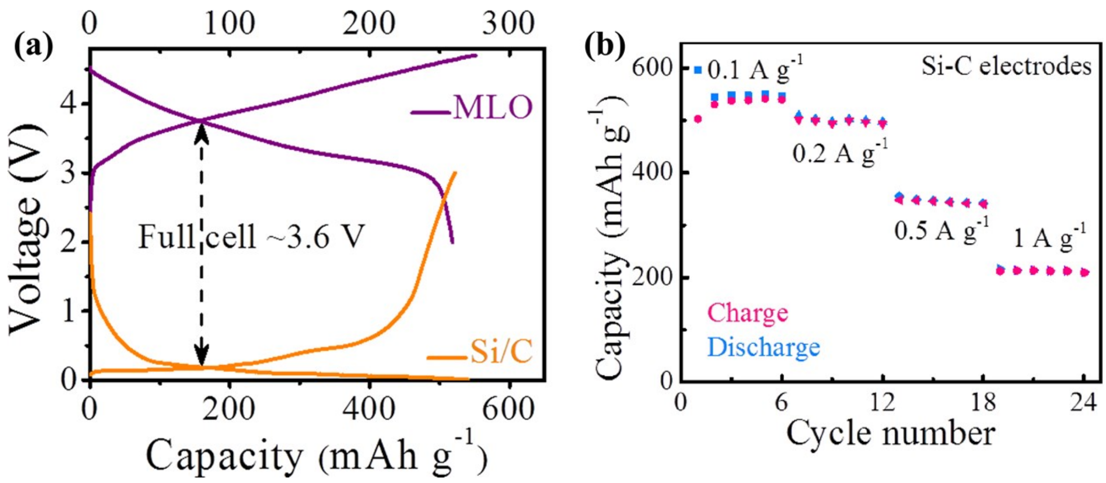

Fig. S10 (a) Charge/discharge profiles for the modified cathode and Si/C anode, and (b) rate capacities of Si/C anode.

The electrochemically pre-lithiated Si/C materials are utilized as the anodes, and its rate capacities exhibited in Fig. S10. The redox potential of the full cell is predicted around 3.6 V (Fig. S10a), and verified by the actual measurements (Fig. 4e). The stability of the full cell operated between 2 V and 4.7 V were shown in Fig. 4f. Rates and capacities are calculated based on the mass of MLO cathode. At 0.1, 0.2, 0.5, 1 and 2 C rate, discharge capacities of 250, 222, 181, 165, and 137 mAh g^{-1} are achieved, respectively. When subsequently switched to 0.2 C, the capacity recovers very well.

References

S1 Qingyuan Li, Dong Zhou, Lijuan Zhang, De Ning, Zhenhua Chen, Zijian Xu, Rui Gao, Xinzhi Liu, Donghao Xie, Gerhard Schumacher, and Xiangfeng Liu. Tuning Anionic Redox Activity and Reversibility for a High-Capacity Li-Rich Mn-Based Oxide Cathode via an Integrated Strategy. Adv. Funct. Mater., 2019, 1806706.

S2 Wei Zhu, Zige Tai, Chengyong Shu, Shaokun Chong, Shengwu Guo, Lijie Ji, Yuanzhen Chen, and Yongning Liu. The superior electrochemical performance of a Li-rich layered cathode material with Li-rich spinel $Li_4Mn_5O_{12}$ and MgF_2 double surface modifications. J. Mater. Chem. A, 2020, 8 (16), 7991-8001.

S3 Qingyuan Li, De Ning, Dong Zhou, Ke An, Deniz Wong, Lijuan Zhang, Zhenhua Chen, Götz Schuck, Christian Schulz, Zijian Xu, Gerhard Schumacher, and Xiangfeng Liu. The Nature of Oxygen Vacancy and Spinel Phase Integration on Both Anionic and Cationic Redox in Li-rich Cathode Material. J. Mater. Chem. A, 2020, DOI: 10.1039/D0TA02517H.

S4 Xu-Dong Zhang, Ji-Lei Shi, Jia-Yan Liang, Ya-Xia Yin, Jie-Nan Zhang, Xi-Qian Yu, and Yu-Guo Guo. Suppressing Surface Lattice Oxygen Release of Li-Rich Cathode Materials via Heterostructured Spinel $Li_4Mn_5O_{12}$ Coating. Adv. Mater., 2018, 30, 1801751.

S5 Gang Sun, Fu-Da Yu, Lan-Fang Que, Liang Deng, Min-Jun Wang, Yun-Shan Jiang, Guangjie Shao, and Zhen-Bo Wang. Local electronic structure modulation enhances operating voltage in Li-rich cathodes. Nano Energy, 2019, 66, 104102.

S6 Pengfei Liu, Hong Zhang, Wei He, Tengfei Xiong, Yong Cheng, Qingshui Xie, Yating Ma, Hongfei Zheng, Laisen Wang, Zi-Zhong Zhu, Yong Peng, Liqiang

Mai, and Dong-Liang Peng. Lithium Deficiencies Engineering in Li-Rich Layered Oxide $Li_{1.098}Mn_{0.533}Ni_{0.113}Co_{0.138}O_2$ for High-Stability Cathode. J. Am. Chem. Soc., 2019, 141, 10876-10882.